Journal of Power Sources 202 (2012) 47–55

Contents lists available at SciVerse ScienceDirect

Journal of Power Sources

journal homepage: www.elsevier.com/locate/jpowsour

Thin film growth of yttria stabilized zirconia by aerosol assisted chemical vapor deposition

M.V.F. Schlupp*, M. Prestat, J. Martynczuk, J.L.M. Rupp, A. Bieberle-Hütter, L.J. Gauckler

Nonmetallic Inorganic Materials, ETH Zürich, Wolfgang-Pauli-Str. 10, 8093 Zürich, Switzerland

ARTICLE INFO

Article history:
Received 29 July 2011
Received in revised form 31 October 2011
Accepted 6 November 2011
Available online 12 November 2011

Keywords:
Thin film deposition
AA-CVD
Deposition mechanism
SOFC electrolyte
YSZ

ABSTRACT

Thin film growth of yttria stabilized zirconia (YSZ) using atmospheric aerosol assisted chemical vapor deposition (AA-CVD) from β-diketonates is studied. The influence of nature and concentration of metal precursors and solvents on thin film growth, microstructure and composition is investigated as a function of deposition temperature. AA-CVD is able to produce smooth and homogeneous YSZ thin films of controlled thickness and stoichiometry. Amorphous, nanocrystalline or columnar microstructures can be obtained at deposition temperatures between 300 and 650 °C. In the same temperature regime, a transition from surface reaction to diffusion controlled film growth is observed. For applications as gas separating membranes, e.g. for micro-solid oxide fuel cell electrolytes, randomly oriented nanocrystalline microstructures with grain sizes in the range of 10 nm are promising.

© 2011 Elsevier B.V. All rights reserved.

1. Introduction

Yttria stabilized zirconia (YSZ) is widely used as electrolyte for anode supported thin film solid oxide fuel cells [1,2] and planar micro-solid oxide fuel cells (μ-SOFCs) [3]. For these applications, the deposition of smooth and homogeneous layers of 50–750 nm thickness is required ([3] and references therein). Processing temperatures of such YSZ thin films should be kept low (e.g. <600 °C) in order to avoid interface reactions and minimize inter-diffusion between substrate and different thin films [4], while still providing stable microstructures at operating temperatures between 350 °C and 550 °C [3]. The application as oxygen conducting electrolyte further requires YSZ thin films to function as gas-separating membranes and avoid gas cross over through pores or pinholes.

Thin film deposition by aerosol assisted chemical vapor deposition (AA-CVD) at atmospheric pressure combines advantages of chemical vapor deposition and spray pyrolysis. This technique was developed in the 1970s and is able to produce oxide, sulphide, and even metal thin films [5–7]. A review on CVD, AA-CVD and related methods like AA-CVD in an electric field [8] or pulsed-pressure metalorganic CVD [9] is given by Choy [10]. Using a simple, non-vacuum spray pyrolysis setup, a gaseous reactive species containing the thin film constituents is produced from a nebulized precursor solution right above a heated substrate. Film growth occurs from the gas phase resulting in smooth thin films of constant thickness over large areas. The aerosol transport system also facilitates the reproducible deposition of multi-element thin films of defined stoichiometry. In literature, the terms pyrosol process [6,7], ultrasonic spray pyrolysis [11,12], spray deposition [13] and others [14] may describe the same technique.

Zirconia and YSZ depositions by atmospheric AA-CVD were first reported based on butoxide [6,7] and pentanedionate precursors [14]. Several recent papers give more details on YSZ film growth using zirconium and yttrium pentanedionate [11,12,15] or tetramethyl-heptanedionate [16,17]. These studies indicate that AA-CVD thin films with variable properties are obtained depending on the deposition conditions. While amorphous YSZ films have been obtained at substrate temperatures as high as 600 °C [16], nanocrystalline microstructures of YSZ with grain sizes between 10 and 30 nm have been reported for temperatures between 300 and 525 °C in other studies [11,12]. Deposition of cubic YSZ with good preferential orientation in the (1 1 1) direction has also been observed [15]. Atmospheric AA-CVD has been applied to prepare thin film solid oxide fuel cells by Meng et al. [18–20]. However, cells based on YSZ electrolytes did not yield theoretical open circuit voltages, which was ascribed to pinholes in the columnar YSZ electrolyte deposited at temperatures between 400 °C and 600 °C.

This indicates that in order to produce reliable YSZ electrolytes for low temperature thin film SOFCs or free-standing micro-SOFC membranes using AA-CVD at atmospheric pressure, it is necessary to optimize the electrolyte microstructure. Therefore, in this study we thoroughly investigate the relevant deposition parameters and their effect on YSZ film growth and microstructure. Notably, the influence of substrate temperature, precursor type and

* Corresponding author. Tel.: +41 44 633 69 85; fax: +41 44 632 11 32.
E-mail address: Meike.Schlupp@mat.ethz.ch (M.V.F. Schlupp).

0378-7753/$ – see front matter © 2011 Elsevier B.V. All rights reserved.
doi:10.1016/j.jpowsour.2011.11.016

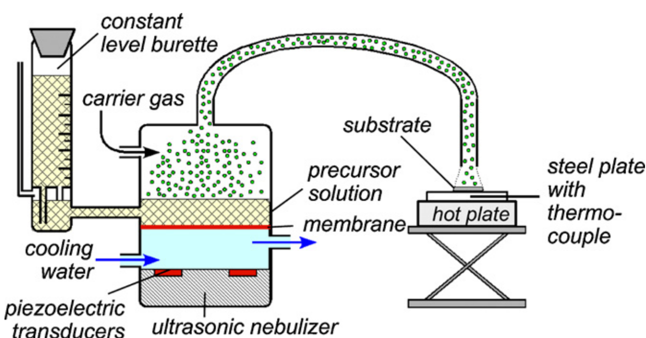

Fig. 1. Experimental setup of ultrasonic aerosol assisted chemical vapor deposition at atmospheric pressure.

concentration, solvent type, and post-deposition treatment on thin film grow rate, microstructure, crystallinity and elemental composition is examined.

2. Experimental

Most AA-CVD experiments in this study were performed using the β-diketonates zirconium 2,4-pentanedionate [$Zr(acac)_4$, 95% purity, ABCR] and yttrium 2,4-pentanedionate [$Y(acac)_3$, 99.9% purity, Alfa Aesar] dissolved in anhydrous ethanol [A15 Alcosuisse, >99.8% purity, boiling point 78 °C] or 50 vol.% anhydrous ethanol + 50 vol.% heptane [Brenntag Schweizerhall AG, boiling point ≈ 98 °C]. Deposition was also performed using zirconium 2,2,6,6-tetramethyl 3,5-heptanedionate [$Zr(tmhd)_4$, 99% purity, Strem Chemicals] and yttrium 2,4-pentanedionate dissolved in ethanol + heptane. Different yttrium:zirconium ratios between 0:1 and 0.4:0.6 with total salt concentrations between 0.005 and 0.025 M were investigated.

The precursor solutions were nebulized in a custom-made spray setup (Fig. 1) based on a commercially available ultrasonic nebulizer (Fogstar 600, Seliger, Germany) with 6 piezoelectric transducers (Ø 20 mm) operating at a frequency of 1.7 MHz. The ultrasonic nebulizer was water cooled by an external cooling cycle at approximately 10 °C, which was separated from the precursor solution by a polyimide membrane of 25 μm thickness. The fill level of the precursor solution was maintained during deposition using a purpose-built constant level burette, which also allowed to monitor the average solution throughput during experiments. The solution throughput in this setup cannot be adjusted directly, but depends on the nebulizer setup and the properties of the precursor solution like solution density and surface tension [21]. The precursor nebula was transported to a heated substrate through a glass tube using filtered air at a flow rate of 4 l min^{-1} as a carrier gas. The distance between tube outlet and substrate was kept at 6 mm for all depositions.

YSZ thin films were deposited on ⟨1 0 0⟩ oriented silicon wafers (ABC, Germany, 500 μm thickness) and randomly oriented sapphire single crystals (Stettler, Switzerland, 500 μm thickness) at substrate temperatures between 300 and 650 °C. To accurately adjust the substrate temperature (T_s), a steel plate equipped with a thermocouple (type K) was placed on the hot plate, and the hot plate temperature was controlled by this thermocouple using a Eurotherm controller. The substrate temperature was measured with an external contact thermocouple, and the hot plate temperature was adjusted accordingly.

Top-view morphologies and film thicknesses of freshly fractured cross sections were characterized using scanning electron microscopy (FEG-SEM, Zeiss LEO Gemini 1530, Germany) with an in-lens detector at 5 kV. Prior to imaging, the samples were coated with a thin platinum coating to avoid charging and to allow imaging at higher resolution. Film thicknesses were determined from the cross sections as an average of at least three sample positions. The average roughness was determined using a Topometrix 2000 atomic force microscope (AFM) in contact mode. Transmission electron microscopy (TEM) investigations were performed on cross-sectional thin film samples deposited on silicon using a FEI Tecnai F-30 (field emission gun) with an accelerating voltage of 300 kV and post-column CCD camera. A traditional sample preparation technique based on polishing, dimpling and ion milling (Gatan precision ion polishing system at 4 keV and 4° angle of incidence from top and bottom) was applied. The phase content was analyzed by X-ray diffraction (XRD, X'pert Pro, Panalytical, Netherlands). The setup was equipped with a copper radiation source operated at 45 kV and 40 mA ($K_{\alpha1}$ = 1.5406Å) using a nickel filter. The average crystallite size of randomly oriented YSZ was derived by multiplying the volume weighted column length determined using the software Topas Academic V4.1 by 4/3 for a spherical shape [22]. The cation composition of YSZ thin films was investigated by X-ray photoelectron spectroscopy (XPS, Sigma2, Thermo Fisher Scientific, UK). All spectra were acquired at 300 W with an AlK_α X-ray source (1486.6 eV) and large area spot size at pressures <10^{-6} Pa. On the basis of survey spectra, the following chemical species were probed with high resolution (0.1 eV step size and 25 eV pass energy): Zr 3d, Y 3d, O 1s, and C 1s. All data were analyzed using the

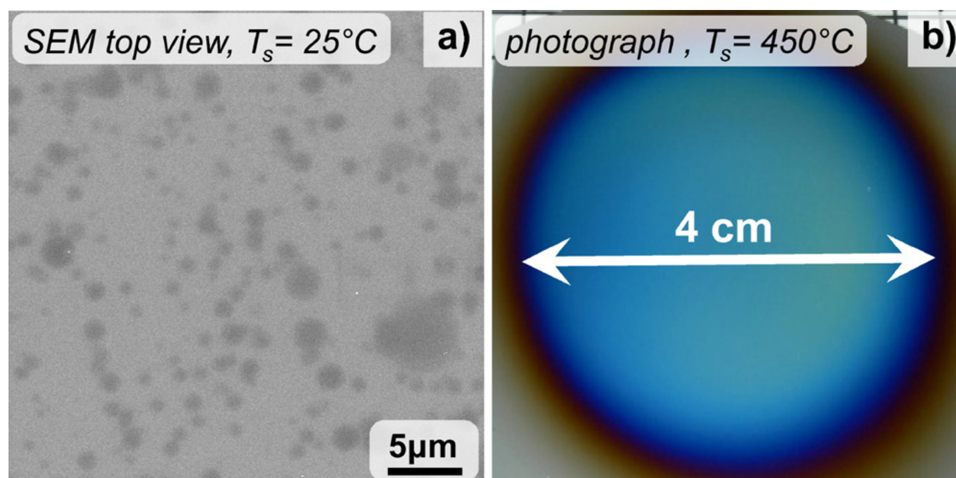

Fig. 2. (a) Deposition by wet droplets at room temperature and (b) typical YSZ thin film by AA-CVD on silicon (T_s = 450 °C) showing blue interference color. (For interpretation of the references to color in this figure legend, the reader is referred to the web version of the article.)

program CasaXPS (V2.3.15, Casa Software Ltd., UK). Prior to fitting of the XPS detailed spectra, an iterated Shirley-Sherwood background subtraction was applied using a linear-least square algorithm, and the spectra were referenced to the aliphatic hydrocarbon C 1s signal at 285.0 eV. The whole peak area of Zr 3d and Y 3d was used to calculate the yttrium:zirconium ratio in the thin films.

3. Results

3.1. YSZ thin film deposition by AA-CVD

Thin film growth by AA-CVD only occurs at elevated temperatures. For room temperature experiments, circular objects in the lower micrometer range can be imaged by SEM after deposition (Fig. 2a). Most of these features have diameters between 0.5 and 1.5 μm, with only few larger ones up to 5 μm. At this low temperature, wet droplets reach the substrate and, after drying, deposit the un-reacted metal precursor. These features therefore are an indication of the droplets size of the aerosol. At low substrate temperatures between 50 °C and 250 °C, no deposits (neither film, particles, nor droplets) are found on the substrates for deposition times up to 60 min.

Thin film deposition is observed for substrate temperatures of 300 °C and above. On silicon substrates, mirror-like YSZ layers are obtained with thickness dependent interference colors, indicating smooth and homogeneous coatings over more than 10 cm^2 (Fig. 2b).

Above 300 °C, increasing film growth rates are obtained for increasing substrate temperatures (Fig. 3). While the growth rates are constant with time, rates of 12 nm min^{-1}, 40 nm min^{-1} and 75 nm min^{-1} are determined for substrate temperatures of 400 °C, 450 °C and 600 °C, respectively. Based on the distribution of interference colors, the thickness of films deposited at high temperatures, e.g. at 600 °C, is less homogenous across the sample than those deposited at lower temperatures, e.g. at 500 °C and below.

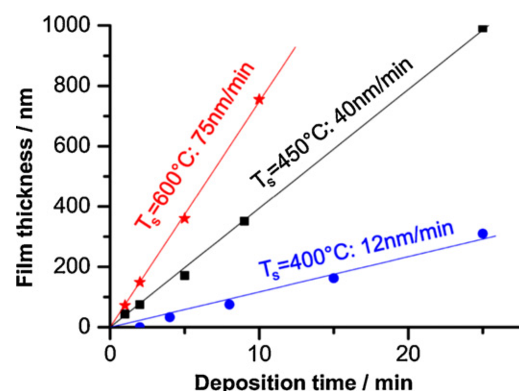

Fig. 3. YSZ growth rates for substrate temperatures T_s of 400, 450 and 600 °C from a solution of 0.025 M $Zr(acac)_4 + Y(acac)_3$ in ethanol.

The deposition conditions also have a strong influence on the resulting film microstructure. As shown in Fig. 4, smooth and homogeneous YSZ layers are obtained for deposition on silicon from 0.025 M $Zr(acac)_4 + Y(acac)_3$ in ethanol at 450 °C. No significant

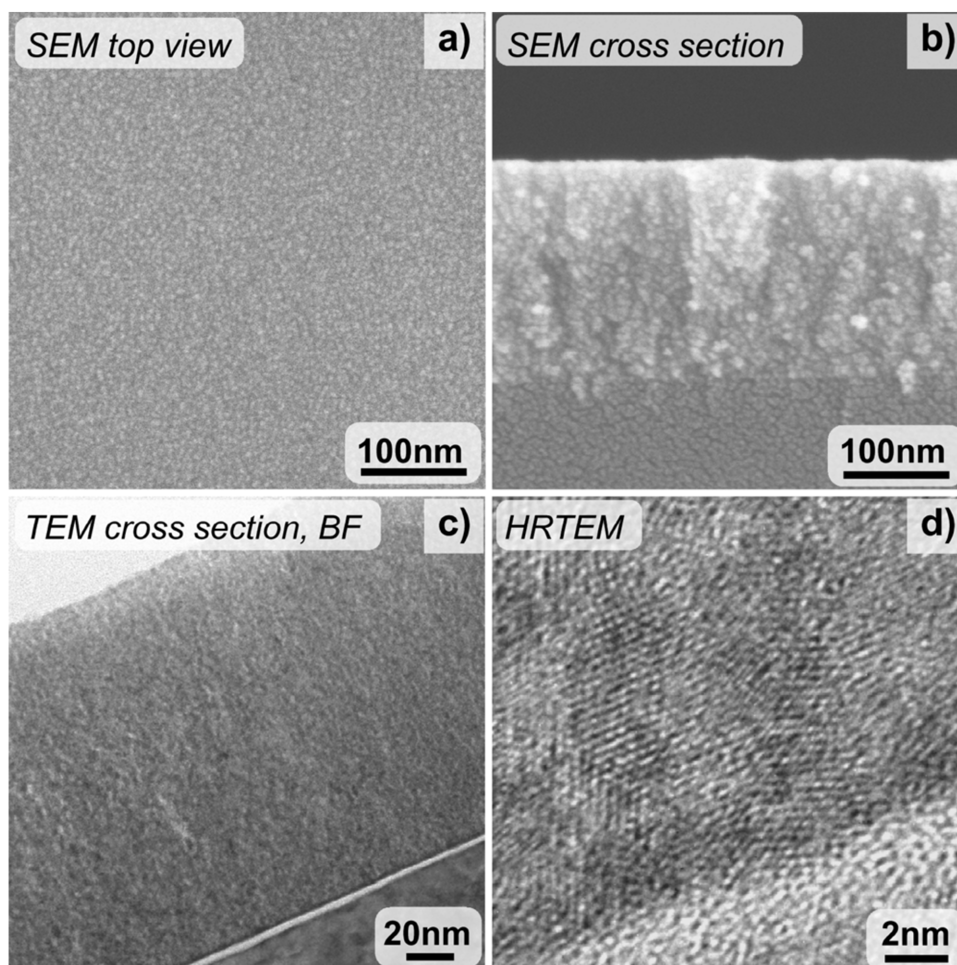

Fig. 4. Nanocrystalline microstructure of YSZ thin films deposited on silicon at 450 °C (0.025 M $Zr(acac)_4 + Y(acac)_3$ in ethanol).

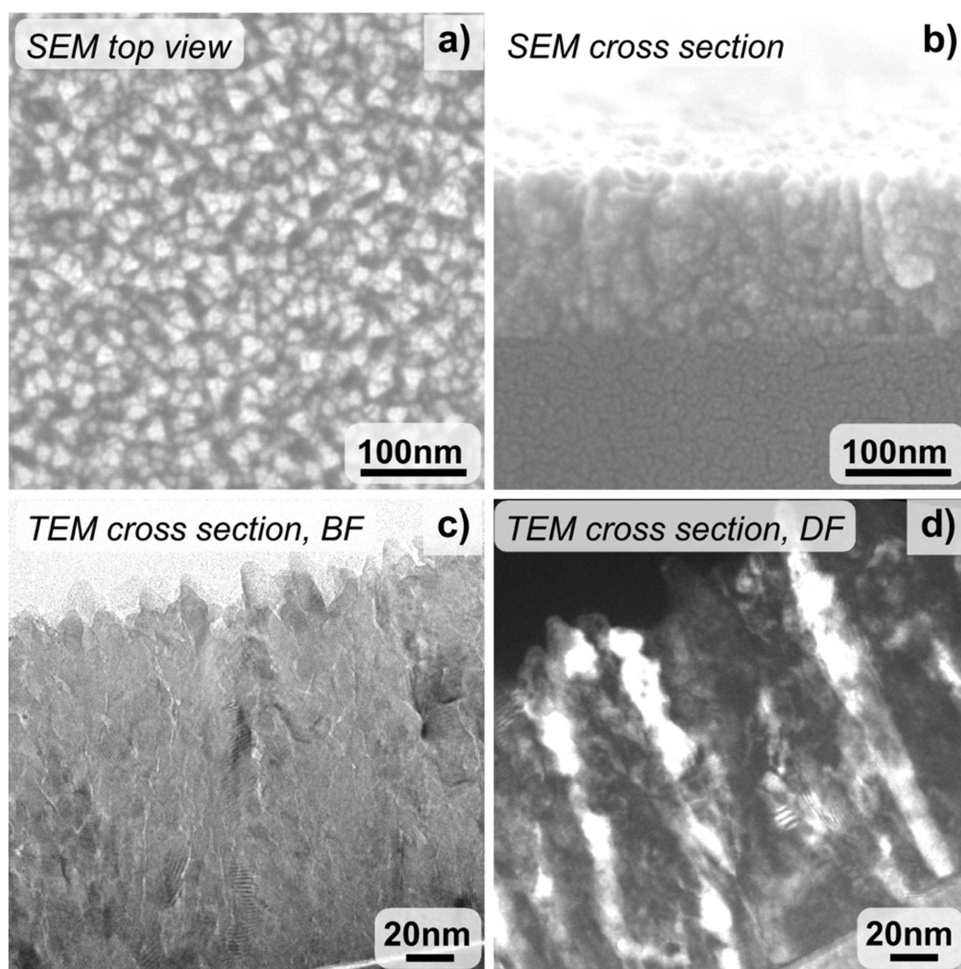

Fig. 5. Columnar microstructure of YSZ thin films deposited on silicon at 600 °C (0.005 M $Zr(acac)_4 + Y(acac)_3$ in ethanol).

features are visible by SEM overview images (Fig. 4a and b), and corresponding AFM measurements yield average roughnesses below 2 nm (not shown). TEM images of the same sample (Fig. 4c and d) reveal that the material consists of randomly oriented nanocrystals with diameters in the range of 5 nm. This nanocrystalline structure is confirmed by selected area diffraction (not shown). For films deposited on silicon, an amorphous interlayer with bright TEM contrast is found between substrate and thin film. This is ascribed to native silicon oxide which has a thickness of few nanometers after deposition.

In contrast, the coatings deposited on silicon from 0.005 M $Zr(acac)_4 + Y(acac)_3$ in ethanol at 600 °C exhibit a granular morphology with pyramidal features around 20 nm in SEM top view images (Fig. 5a). Corresponding bright field (BF) and dark field (DF) TEM images (Fig. 5c and d) reveal a skewed, but columnar microstructure with crystals stretching from the bottom to the top of the thin film. This structure is hardly visible in cross sectional SEM images (Fig. 5b), which show the morphology of the fracture surface.

This temperature and concentration dependent change in microstructure can also be observed by X-ray diffraction (Figs. 6 and 7), which reveals a cubic (or tetragonal) zirconia phase for all samples deposited at and above 400 °C. All films grown at 300 °C are XRD amorphous (not shown). Similar results are obtained for deposition on sapphire and silicon substrates. For deposition from a 0.025 M solution (Fig. 6), randomly oriented structures are obtained for substrate temperatures of 450 °C and 600 °C. The XRD crystallite size of the nanocrystalline material deposited at 450 °C is 3–4 nm, which corresponds well to the results of HRTEM in Fig. 4d. The crystallite size obtained from 0.025 M at 600 °C is around 10 nm. For deposition from a 0.005 M solution (Fig. 7), the films show a preferred (1 1 1) orientation for substrate temperatures of 600 °C (corresponding to the microstructures in

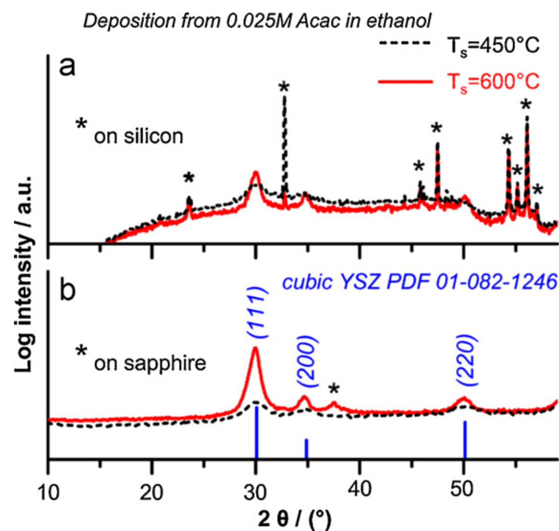

Fig. 6. Influence of substrate nature and temperature on XRD patterns of YSZ thin films. Deposition from 0.025 M $Zr(acac)_4 + Y(acac)_3$ in ethanol on (a) silicon and (b) sapphire substrates. (*h k l*) indices of cubic YSZ; *XRD signals of silicon and sapphire substrate, respectively.

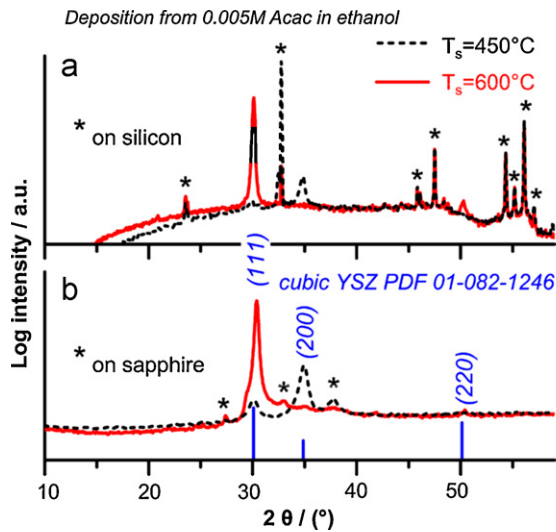

Fig. 7. Influence of substrate nature and temperature on XRD patterns of YSZ thin films. Deposition from 0.005 M $Zr(acac)_4 + Y(acac)_3$ in ethanol on (a) silicon and (b) sapphire substrates. (*h k l*) indices of cubic YSZ; ∗XRD signals of silicon and sapphire substrate, respectively.

Fig. 5). For deposition at 450 °C, the (1 0 0) orientation is more pronounced.

The randomly oriented vs. columnar character formed during deposition is preserved on post-deposition annealing at 600 °C for 20 h. However, a decrease in full-width-at-half-maximum of XRD patterns is observed for samples deposited at 450 °C and 600 °C from a 0.025 M solution (not shown). For the randomly oriented material deposited at 450 °C, a crystallite size of approximately 8 nm is obtained after annealing. The corresponding TEM cross sections (Fig. 8) also indicate an increase in crystallinity of the material after annealing (compare to Fig. 4).

3.2. Cation transfer from solution to thin film

As different metal precursors often exhibit different growth rates in chemical vapor deposition, the yttrium to zirconium ratio of thin films produced under varying process conditions was measured by XPS. The actual cation concentration of the yttrium and zirconium precursors was determined by thermogravimetry (not shown). Precursor solutions containing 0–40 at.% of yttrium (relative to zirconium) and total metal concentrations of 0.005–0.02 M were prepared using ethanol as a solvent. Thin films were deposited at substrate temperatures between 450 and 600 °C using carrier gas flows of 2 and 4 Nl min^{-1}. Fig. 9 shows the yttrium content of these thin films compared to that of their corresponding precursor solutions. Less yttrium than present in the precursor solutions is incorporated in the thin films. However, the same transfer ratio is obtained for all process parameters applied. As determined by a linear fit of all data, the yttrium transfer ratio from solution to thin film is 0.79 ± 0.02 in our region of interest between 0 and 30% yttrium. According to this, precursor solutions containing 20 at.% of yttrium should be used to deposit 8YSZ ($Zr_{0.84}Y_{0.16}O_{2-\delta}$).

The yttrium transfer ratio is also found to be independent of the substrate material (sapphire, silicon, or silicon nitride coated silicon), and of deposition times between 5 and 30 min corresponding to film thicknesses between 50 and 270 nm (not shown). There is, however, a strong influence of the precursor solution temperature in the nebulizer. The yttrium transfer ratio decreases to 0.54 for a sample deposited with the water cooling switched off, to even 0.13 after further warming of the precursor solution in the ultrasonic nebulizer.

3.3. YSZ film growth kinetics

For a closer study on the temperature dependence of AA-CVD film growth, depositions were performed in 33 °C steps between 300 and 633 °C for different precursor solutions. YSZ film growth from different metal precursors [$Zr(acac)_4$+$Y(acac)_3$ vs. $Zr(tmhd)_4$+$Y(acac)_3$], metal concentrations [0.005 M vs. 0.025 M], and solvent systems [pure ethanol vs. heptane + ethanol] was investigated. Based on the yttrium transfer rate for 2,4-pentanedionates, solutions containing 20 at.% yttrium and 80 at.% zirconium were applied. Film growth of un-doped zirconia was also studied.

Fig. 10a shows the film growth rates of two spray solutions with different metal precursor concentrations, which are based on zirconium and yttrium 2,4-pentanedionates dissolved in pure ethanol. In addition, the growth rates of the same precursors dissolved in a mixture of heptane and ethanol at 0.005 M are shown.

Between 300 and 400 °C, the growth rates are independent of the precursor concentration and choice of solvent. They show the same, Arrhenius-type dependence on the deposition temperature with apparent activation energies of 76 ± 20 kJ mol^{-1}. At higher temperatures, the growth rates are strongly influenced by the precursor concentration, but show only weak dependence

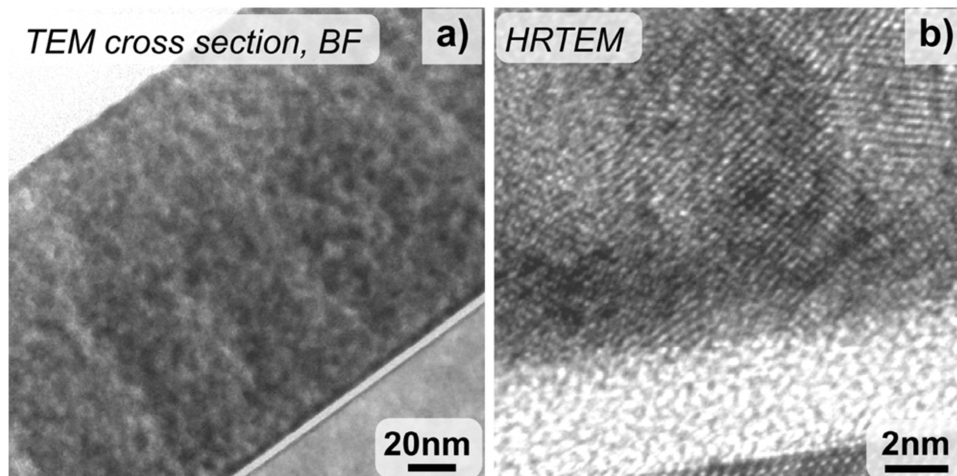

Fig. 8. Conservation of nanocrystalline microstructure of YSZ thin films deposited on silicon at 450 °C after annealing at 600 °C for 20 h (0.025 M $Zr(acac)_4 + Y(acac)_3$ in ethanol).

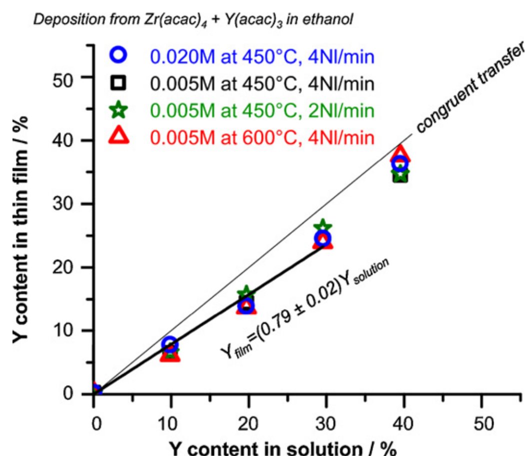

Fig. 9. Yttrium transfer from solution to thin film as measured by XPS. A constant yttrium transfer ratio of 0.8 is obtained for varying process parameters.

on the substrate temperature. At and above 500 °C, growth rates around 60 nm min^{-1} are obtained for ethanol solutions with metal concentrations of 0.025 M, while growth rates of approximately 7 nm min^{-1} are obtained for concentrations of 0.005 M between 433 and 633 °C. A very similar behavior of growth rates is also found for deposition of pure ZrO_2 from $Zr(acac)_4$ in ethanol. While the same thermally activated regime is found at lower temperatures, slightly higher growth rates than for YSZ are obtained in the high temperature regime (not shown). Besides the metal precursor concentration, the type of solvent also has an influence on YSZ growth rates above 400 °C. For the same metal concentration of 0.005 M, the deposition rates double from roughly 7 nm min^{-1} for pure ethanol solutions to about 15 nm min^{-1} for ethanol + heptane as solvent (Fig. 10a). At the same time, the precursor solution throughput of the ultrasonic nebulizer unit is about twice as high for ethanol + heptane (4.9 ml min^{-1} on average) than for pure ethanol solutions (2.5 ml min^{-1}). The average solution throughput of the ultrasonic nebulizer does not depend on the dissolved precursor salts.

In contrast to films deposited from 2,4-pentanedionates, the growth rates based on $Zr(tmhd)_4$ show a higher temperature dependence in the upper temperature regime (Fig. 10b). Two regimes with different activation energies can be identified for temperatures below and above 450 °C. At low temperatures, the apparent activation energy of 72 ± 16 kJ mol^{-1} is similar to that of the pentanedionate precursors. The growth rates of the tetramethyl-heptanedionate solution are, however, by a factor of two lower in this regime. Above 450 °C, a second thermally activated process with E_a = 30 ± 2 kJ mol^{-1} can be identified with good accuracy. As a consequence, the growth rates reach those of 0.005 M pentanedione in ethanol + heptane around 600 °C.

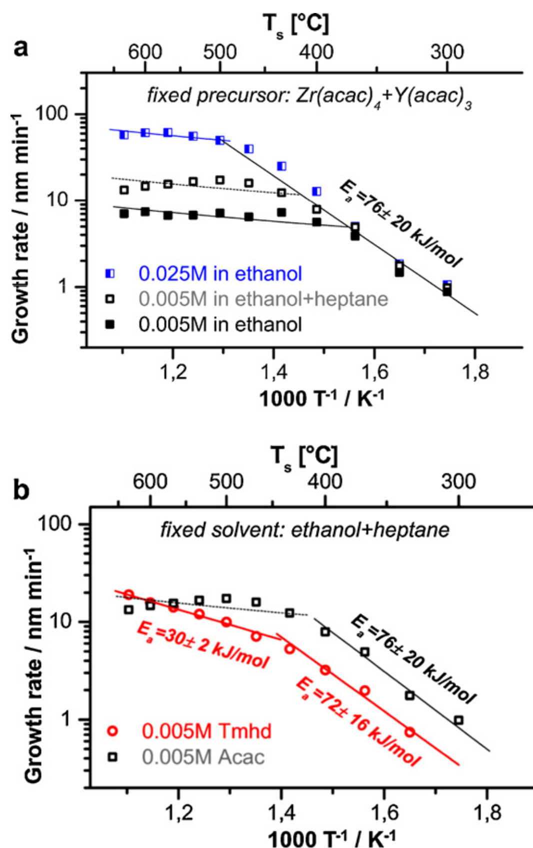

Fig. 10. Influence of (a) metal precursor concentration and solvent system and (b) type of metal precursor on thin film growth rates and apparent activation energies of YSZ film growth. The average solution throughput determined for all ethanol solutions was 2.5 ml min^{-1}, while that for all ethanol + heptane solutions was 4.9 ml min^{-1}.

4. Discussion

4.1. YSZ thin film deposition and microstructure

Thin film deposition of YSZ is only possible at temperatures at and above 300 °C in our experiments. Between room temperature and approximately 100 °C, solution droplets reach the substrate according to a wet spray pyrolysis deposition mechanism. However, with the temperatures being so low, no decomposition of the metal precursor occurs. Between 100 °C and 300 °C, no deposits are found on the substrate at all. In this regime, the ethanol solvent evaporates well above the substrate, leaving finely divided metal precursor precipitates in the gas stream. However, thermophoretic forces drive the particles away from the hot substrate [23], and the particles are vented away with the gas flow. At and above 300 °C, film growth by chemical vapor deposition occurs. This minimal film growth temperature was also reported for the deposition of zirconia by rapid thermal CVD from Zr-t-butoxide with oxygen under reduced pressure [24].

In the CVD regime, film microstructures depend on substrate temperature and precursor concentration, and are thereby influenced by the film growth rate. This is due to an interplay between nucleation and growth kinetics during deposition [10], which are in turn influenced by the precursor supersaturation and mobility of adsorbed precursor species on the substrate surface. At very low deposition temperatures, e.g. at 300 °C, the mobility of adsorbed precursor species on the substrate surface is so low that nucleation occurs without detectable grain growth, and amorphous deposits are obtained. At intermediate temperatures, e.g. 450 °C, both nucleation and grain growth occur. At this temperature, the different precursor concentrations in ethanol correspond to growth rates of roughly 7 nm min^{-1} for the 0.005 M solution and 40 nm min^{-1} for the 0.025 M solution. The different growth rates also influence the resulting microstructure (Figs. 6 and 7). While randomly oriented nanocrystals are obtained for deposition at 40 nm min^{-1}, slightly larger crystallites with some degree of preferred orientation in (1 0 0) are obtained for the slower growth rate. This reflects the migration of gaseous reactants to preferred lattice sites corresponding to the fast growing (1 0 0) planes. At even higher temperatures, e.g. 600 °C, surface diffusion is high enough to allow migration of precursor molecules to the (1 1 1) lattice planes of lowest surface energy for slow deposition. Columnar grains are obtained from 0.005 M solutions (growth rate around 7 nm min^{-1}) on both

sapphire and silicon. For fast deposition from 0.025 M solutions (roughly 70 nm min^{-1}), more randomly oriented crystals are again obtained.

The film thickness increases linearly with deposition time at all temperatures, and continuous films have been produced with thicknesses down to the detection limit of SEM (approximately 15 nm). In our experiments, film growth occurs on off-axis oriented crystalline sapphire substrates and on silicon wafers. The substrate surface of silicon is amorphous, because native silicon oxide grows to several nanometers thickness at the elevated substrate temperatures. No significant influence of the substrate material was observed for YSZ film growth. However, diffusion of silicon to YSZ grain boundaries may impede grain growth on silicon substrates at temperatures as low as 600 °C [4].

4.2. Cation transfer from solution to thin film

The ability to deliver a spray of fixed metal precursor ratio and concentration is advantageous in AA-CVD as compared to conventional CVD, because it allows reproducible deposition of multi-elemental thin films with constant composition. In our study, an yttrium transfer ratio of 0.8 is always obtained for a fixed choice of metal precursors [$Zr(acac)_4$ + $Y(acac)_3$] and solvent [ethanol]. This ratio is constant for different process parameters like substrate choice, deposition time, deposition temperature, total metal precursor concentration, and carrier gas flow. It is thus also not influenced by the film growth rate. However, the temperature of the spray solution in the nebulizer does have a strong influence on the yttrium transfer. In our setup, both the ultrasonic nebulizer unit and the precursor solution are water cooled. This is done to assure a transport of the precursor solution (in form of an aerosol) at room temperature. Because the vaporization of metal precursors occurs only directly above the heated substrate, very reproducible transfer ratios are obtained. The literature available on yttrium transfer in AA-CVD of YSZ holds differing results. Based on the same $Zr(acac)_4$ + $Y(acac)_3$ precursors dissolved in methanol with varying concentrations, Ramirez et al. [12] obtained values scattered around a congruent yttrium transfer (transfer ratio = 1) for deposition at 525 °C. Similarly, an (almost) congruent transfer was reported by Wang et al. [15] for one composition of 0.05 M $Zr(acac)_4$ + $Y(acac)_3$ in dimethylformamide (DMF) at 550 and 700 °C. This, however, changed drastically for a deposition temperature of 450 °C, where a transfer ratio of only 0.19 was obtained.

For AA-CVD deposition from $Zr(tmhd)_4$ and $Y(tmhd)_3$ in toluene, Song et al. [16] report a constant transfer ratio of 0.92 in the substrate temperature range of 400–600 °C. The same group also obtained ratios of 0.84 at 600 °C and 0.82 at 800 °C for the same materials but slightly different experimental settings [25]. After the addition of halogen lights between nozzle and sample holder, preferential incorporation of yttrium was observed at 650 °C with a transfer ratio of 2.30 using the same solutions as before [17]. This was explained by a change in the rate limiting deposition mechanism caused by higher temperatures in the gas phase above the substrate. Besides the solution and aerosol temperature, the exact experimental setup and especially the temperature distribution above the heated substrate therefore have a significant influence on the cation transfer. This makes AA-CVD cation transfer ratios reported in literature difficult to compare.

4.3. Film growth processes in aerosol assisted CVD

Most of the literature data on zirconia and YSZ film growth by metal organic chemical vapor deposition (MOCVD) [26–30] and AA-CVD [11,16,25,31] show a transition from a thermally activated regime at low temperatures to a regime with weak temperature dependence at high temperatures as observed in Fig. 10. For MOCVD, there is a huge scatter of reported data with growth rates between 10 and 1000 nm min^{-1} and apparent activation energies (E_a) between 50 kJ mol^{-1} [26] and 150 kJ mol^{-1} [28] in the low temperature regime. For AA-CVD, growth rates from several to 100 nm min^{-1} are reported with apparent activation energies between 30 kJ mol^{-1} [16] and 60 kJ mol^{-1} [11].

The dependence of film growth rates on process parameters can be used to identify the processes limiting deposition [10,23,32]. The different rate limiting regimes applicable to AA-CVD are discussed in the following. Fig. 11 shows a schematic sketch of deposition processes in AA-CVD together with the dependence of gaseous species and temperature on their distance to the substrate surface.

4.3.1. Feed rate limited deposition

In AA-CVD, the feed rate is a result of (I.i) aerosol delivery to the reaction zone and (I.ii) vaporization of the metal precursor [23] (Fig. 11).

Aerosol delivery (I.i) is determined by the properties of the aerosol (flow rate, droplet size, etc.) and the spray solution (e.g. chemical composition and precursor concentration). Because the aerosol delivery rates by ultrasonic nebulizers are quite high, delivery limited deposition can usually be avoided [23]. In our setup, aerosol delivery corresponds to the precursor solution throughput, which can be used to estimate the efficiency of precursor conversion. It is around 4% for 0.005 M ethanol and 4.5% for ethanol + heptane solutions, while 7% are obtained for 0.025 M ethanol solutions. Aerosol delivery is therefore not expected to limit film growth. Furthermore, the thermally activated regime obtained for deposition from heptanedionate ($E_a = 30 \pm 2$ kJ mol^{-1}) cannot be explained by limitation through aerosol delivery.

Precursor vaporization (I.ii) depends mainly on the choice of metal precursor and the temperature regime. Close to the heated substrate, where the temperature is increased to the vaporization temperature T_v, the low boiling point solvent of the aerosol droplets evaporates, and the metal precursor is vaporized. Its evaporation rate v is related to temperature in an Arrhenius type behavior, where the thermal activation energy E_a can be approximated by the vaporization enthalpy ΔH_v of the precursor [33], and v_0 and R have their usual meanings:

$$v = v_0\, e^{-(\Delta H_v / R T_v)}. \quad (1)$$

Precursor vaporization limited deposition has been reported for the deposition of copper at 140 °C, which showed a dependency on the temperature of a preheating zone (40–80 °C) for the nebulized precursor [34]. The vaporization enthalpy ΔH_v of $Zr(acac)_4$ as determined by differential scanning calorimetry is around 132 kJ mol^{-1} [35], while the activation energy measured for evaporation of $Zr(tmhd)_4$ from a crucible is 107 kJ mol^{-1} [36]. These values do not correspond to the apparent activation energies obtained for the pentanedionate and heptanedionate precursors in Fig. 10. For our experiments, film growth limitations due to insufficient precursor feed rates are therefore not expected.

4.3.2. Gas phase diffusion limited deposition

Once in the reaction chamber, both the transport of the gaseous precursor to, and of gaseous reaction by-products away from the substrate surface have to be considered. To assess these diffusion processes, it is generally assumed that the total resistance to mass transport is contained within a relatively thin layer of gas adjacent to the substrate surface [32] (see Fig. 11).

For dilute non-polar gases, the dependence of the diffusion coefficient on the diffusion temperature T_d can be approximated using the Chapman–Enskog theory [37], where

$$D \propto T_d^{3/2}. \quad (2)$$

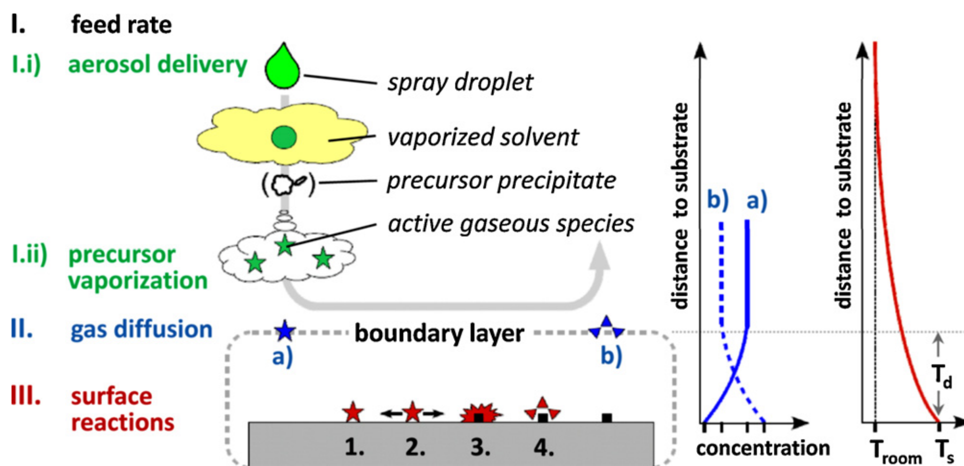

Fig. 11. Schematic representation of deposition processes in substrate heated AA-CVD. The (I) feed rate is determined by (I.i) aerosol delivery and (I.ii) precursor vaporization. Gas phase diffusion (II) implies the transport of (a) active gaseous species to, and of (b) reaction by-products away from the substrate surface through a concentration boundary layer. Surface reactions (III) include (1) adsorption, (2) surface diffusion, (3) chemical reaction, lattice formation, (4) desorption. The concentration of (a) reactant gas and (b) by-products as well as the temperature forms a gradients above the hot substrate.

This dependence on temperatures is rather weak, especially when plotted in an Arrhenius diagram. The gas phase diffusion limited regime is typical for high temperatures and high pressures corresponding to high surface reaction rates and slow diffusion. At atmospheric pressure, the concentration gradient within the boundary layer is decreased and mass transport is slowed down. Diffusion processes in the gas phase are therefore expected to play an important role in AA-CVD. While the deposition rates are high in this regime, non-uniform coatings may result due to local precursor depletion [10].

In fact, the high temperature film growth rates from all solutions in this study could be explained by diffusion limited deposition. Although the gas diffusion temperature T_d forms a gradient above the substrate (Fig. 11) and is not known for our experiments, it is assumed to be lower than the substrate temperature T_s by a constant value ΔT as a first approximation: $T_d = T_s - \Delta T$. The line fits inserted in the high temperature regime of pentanedionate deposition in Fig. 10a correspond to Chapman–Enskog diffusion with growth rates proportional to $(T_s - \Delta T)^{3/2}$. However, due to the limited accuracy of the experimental data, it is not possible to uniquely determine ΔT. The larger growth rates for higher precursor concentration and enhanced droplet delivery (through the higher nebulization rate of the heptane + ethanol solution) can then be explained by enhanced diffusion through an increased concentration gradient according to Fick's first law. As a result of local precursor depletion, the thickness of coatings deposited from pentanedionate precursors does become more inhomogeneous at high substrate temperatures.

For the $Zr(tmhd)_4$ based solution, a higher apparent activation energy of 30 ± 2 kJ mol^{-1} is determined above approximately 450 °C. This value is in excellent agreement with the results on AA-CVD deposition from $Zr(tmhd)_4$ and $Y(tmhd)_3$ in toluene obtained by Song et al. [16], who report an activation energy of 31 kJ mol^{-1} for film growth due to diffusion limitations. The deviation from the Chapman–Enskog theory could be due to the different diffusion behavior of the larger tetramethyl-heptanedionate molecules, leading again to an Arrhenius-type dependence on temperature.

Based on these observations, we suggest a diffusion limited regime for the high temperature depositions of our experiments.

4.3.3. Surface reaction limited deposition

The surface reactions comprise several highly temperature dependent processes: (1) adsorption of the gaseous precursor, (2) surface diffusion, (3) chemical reaction and lattice formation, and (4) desorption of gaseous reaction by-products. Generally, the rate constant k of a chemical reaction is considered to have an Arrhenius-type dependence on temperature [38], which corresponds to the substrate temperature T_s in this case.

Overall deposition is often limited by surface reactions at low substrate temperatures and slow reaction rates. While the deposition rates are low, abundant reactants are available near the substrate surface. This enables the deposition of films of uniform thickness.

The thermally activated regimes between 300 and 400 °C in Fig. 10 show the same apparent activation energy of 76 ± 20 kJ mol^{-1} for different solvents and different precursor concentrations and are assigned to surface reaction limitation. The fact that the same activation energy is also obtained for the two different β-diketonate precursors suggests that YSZ lattice formation (3) is the rate limiting step. The decreased absolute growth rate of the tetramethyl-heptanedionate precursor as compared to pentanedionates in the low temperature regime could be due to the larger size of the $Zr(tmhd)_4$ molecules. Because of their bulky ligands, a lower density of adsorbed species is obtained on the substrate surface, which leads to lower growth rates.

5. Conclusions

Based on a detailed understanding of the deposition mechanism, thin film growth by chemical vapor deposition can be obtained using a simple, non vacuum ultrasonic nebulizer setup. In this study, smooth and homogeneous YSZ films are produced at substrate temperatures between 300 and 650 °C. Depending on the deposition temperature, amorphous, nanocrystalline, or columnar microstructures develop. For our deposition conditions, the yttrium transfer ratio from solution to thin film for $Zr(acac)_4 + Y(acac)_3$ in ethanol is 0.8 for varying process parameters. The desired cation composition can be obtained by adjusting the composition of the precursor solution.

The thin film growth rates are influenced by deposition temperature and solution composition. At low temperatures (300–400/500 °C depending on the precursor concentration), film growth is limited by surface reactions: similar apparent activation energies in the range of 70 or 80 kJ mol^{-1} are obtained for pentanedionate and tetramethyl-heptanedionate precursors. At higher substrate temperatures (above 400/500 °C), deposition becomes gas phase diffusion limited. For $Zr(acac)_4 + Y(acac)_3$, growth rates are proportional to $T^{3/2}$ according to the Chapman–Enskog theory;

for the tetramethyl-heptanedionate precursor, an apparent activation energy of $30 \pm 2\,\mathrm{kJ\,mol^{-1}}$ is obtained.

For application as gas tight electrolytes, the randomly oriented nanocrystalline YSZ thin films obtained by AA-CVD at intermediate temperatures (e.g. 450 °C) and fast deposition rates are promising. For this purpose, further studies will be conducted to evaluate the gas tightness and electrical conductivity of the films. Furthermore, the thermomechanical stability of free standing membranes will be investigated.

Acknowledgements

The authors warmly thank the Laboratory for Surface Science and Technology and the Electron Microscopy Center of ETH Zürich (EMEZ) for support and the use of their XPS and TEM facilities, respectively. Financial support by the following institutions is gratefully acknowledged: Swiss National Science Foundation project CRSI22-126830, Center of Competence Energy and Mobility Switzerland (CCEM), Swiss Electric Research (SER), Competence Centre for Materials Science and Technology Switzerland (CCMX), Korean-Swiss Science and Technology Cooperation.

References

[1] H.-S. Noh, J.-W. Son, H. Lee, H.-S. Song, H.-W. Lee, J.-H. Lee, J. Electrochem. Soc. 156 (2009) B1484–B1490.
[2] T. Van Gestel, D. Sebold, W.A. Meulenberg, H.-P. Buchkremer, Solid State Ionics 179 (2008) 428–437.
[3] A. Evans, A. Bieberle-Hütter, J.L.M. Rupp, L.J. Gauckler, J. Power Sources 194 (2009) 119–129.
[4] B. Scherrer, A. Rossi, J. Martynczuk, M.D. Rossell, A. Bieberle-Hütter, J.L.M. Rupp, R. Erni, L.J. Gauckler, J. Power Sources 196 (2011) 7372–7382.
[5] J.C. Viguie, J. Spitz, J. Electrochem. Soc. 122 (1975) 585–588.
[6] M. Langlet, J.C. Joubert, in: C.N.R. Rao (Ed.), Chemistry of Advanced Materials, vol. XVI, Blackwell Scientific Publications, Oxford, 1993.
[7] G. Blandenet, M. Court, Y. Lagarde, Thin Solid Films 77 (1981) 81–90.
[8] K.L. Choy, W. Bai, B.C.H. Steele, in: 5th International Symposium on Solid Oxide Fuel Cells, Electrochem. Soc. Ser. 97 (1997) 1177–1182.
[9] L. Ramirez, M.L. Mecartney, S.P. Krumdieck, J. Mater. Res. 23 (2008) 2202–2211.
[10] K.L. Choy, Prog. Mater. Sci. 48 (2003) 57–170.
[11] M.F. García-Sánchez, J. Peña, A. Ortiz, G. Santana, J. Fandiño, M. Bizarro, F. Cruz-Gandarilla, J.C. Alonso, Solid State Ionics 179 (2008) 243–249.
[12] E.B. Ramirez, A. Huanosta, J.P. Sebastian, L. Huerta, A. Ortiz, J.C. Alonso, J. Mater. Sci. 42 (2007) 901–907.
[13] A. Ortiz, J. Alonso, E. Haro-Poniatowski, J. Electron. Mater. 34 (2005) 150–155.
[14] Y.M. Gao, P. Wu, R. Kershaw, K. Dwight, A. Wold, Mater. Res. Bull. 25 (1990) 871–876.
[15] H.B. Wang, C.R. Xia, G.Y. Meng, D.K. Peng, Mater. Lett. 44 (2000) 23–28.
[16] H. Song, C. Xia, Y. Jiang, G. Meng, D. Peng, Mater. Lett. 57 (2003) 3833–3838.
[17] Y. Jiang, J. Gao, M. Liu, Y. Wang, G. Meng, Solid State Ionics 177 (2007) 3405–3410.
[18] G.Y. Meng, H.Z. Song, H.B. Wang, C.R. Xia, D.K. Peng, Thin Solid Films 409 (2002) 105–111.
[19] G. Meng, H. Song, Q. Dong, D. Peng, Solid State Ionics 175 (2004) 29–34.
[20] G. Meng, H. Song, C. Xia, X. Liu, D. Peng, Fuel Cells 4 (2004) 48–55.
[21] R.J. Lang, J. Acoust. Soc. Am. 34 (1962) 6–8.
[22] P. Whitfield, L. Mitchell, Int. J. Nanosci. 3 (2004) 757–763.
[23] T. Kodas, M.J. Hampden-Smith, The Chemistry of Metal CVD, VCH, 1994.
[24] J.P. Chang, Y.-S. Lin, K. Chu, J. Vac. Sci. Technol. B 19 (2001) 1782–1787.
[25] Y. Jiang, H. Song, J. Gao, G. Meng, J. Electrochem. Soc. 152 (2005) C498–C503.
[26] R. Tu, T. Kimura, T. Goto, Surf. Coat. Technol. 187 (2004) 238–244.
[27] G. Wahl, W. Nemetz, M. Giannozzi, S. Rushworth, D. Baxter, N. Archer, F. Cernuschi, N. Boyle, J. Eng. Gas Turbines Power 123 (2001) 520–524.
[28] M. Pulver, W. Nemetz, G. Wahl, Surf. Coat. Technol. 125 (2000) 400–406.
[29] S.-C. Hwang, H.-S. Shin, J. Am. Ceram. Soc. 82 (1999) 2913–2915.
[30] G. Garcia, J. Casado, J. Llibre, A. Figueras, J. Cryst. Growth 156 (1995) 426–432.
[31] G. Reyna-Garcia, M. Garcia-Hipolito, J. Guzman-Mendoza, M. Aguilar-Frutis, C. Falcony, J. Mater. Sci. – Mater. Electron. 15 (2004) 439–446.
[32] W.A. Bryant, J. Mater. Sci. 12 (1977) 1285–1306.
[33] J.P. Hirth, G.M. Pound, J. Phys. Chem. 64 (1960) 619–626.
[34] C. Roger, T.S. Corbitt, M.J. Hampdensmith, T.T. Kodas, Appl. Phys. Lett. 65 (1994) 1021–1023.
[35] J.P. Murray, J.O. Hill, Thermochim. Acta 109 (1987) 391–396.
[36] I.E. Korsakov, A.R. Kaul, L. Klippe, J. Korn, U. Krause, M. Pulver, G. Wahl, Microelectron. Eng. 29 (1995) 205–208.
[37] E.L. Cussler, Diffusion: Mass Transfer in Fluid Systems, 2nd edition, Cambridge University Press, 1997.
[38] IUPAC, Compendium of Chemical Terminology (the "Gold Book"), 2nd edition, 1997.